**Environmental Health Engineering and Management Journal 2023, 10(3), 321–329**
http://ehemj.com
doi 10.34172/EHEM.2023.36

Environmental Health
Engineering and
Management Journal

Original Article

Open Access
Publish Free

# Sulfation of metal-organic framework (MOF) nanocatalyst for esterification of oleic acid with methanol to produce biodiesel

**Mahsa Oghabi[1,2], Mohammad Rostamizadeh[1,2*]**

[1]Faculty of Chemical Engineering, Sahand University of Technology, Sahand New Town, Tabriz, Iran
[2]Research Center of Environmental Engineering, Sahand University of Technology, Sahand New Town, Tabriz, Iran

**Abstract**

**Background:** Metal-organic frameworks (MOFs) represent tremendous potential as heterogeneous catalyst in renewable energy production. In this study, biodiesel production using the modified MOF nanocatalyst was investigated in the esterification reaction.

**Methods:** MOF nanocatalyst was prepared using solvothermal method and modified through sulfation process. The nanocatalysts was characterized by XRD, FT-IR, FE-SEM, TEM, $N_2$ adsorption-desorption, and $NH_3$-TPD techniques. The performance of the nanocatalysts was evaluated in the esterification reaction of free fatty acid (FFA) at different operating conditions.

**Results:** The results showed the high crystallinity, appropriate textural properties (995.6 $m^2g^{-1}$), well-adjusted acidity, and high hydrophobicity. The sulfation degree of 4 cc $g^{-1}$ resulted in the best nanocatalyst, which led to the highest FFA conversion (97%) at the optimal conditions: methanol to FFA ratio of 10:1, 3wt.% nanocatalyst, 160 °C, and 6 hours. Surprisingly, the developed nanocatalyst had a great reusability while the conversion reduction was only 8% after six sequence cycles.

**Conclusion:** These results proved the high capability of the developed nanocatalyst in the esterification reaction to produce biodiesel.

**Keywords:** Esterification, Methanol, Fatty acids, Metal-organic frameworks

**Citation:** Oghabi M, Rostamizadeh M. Sulfation of metal-organic framework (MOF) nanocatalyst for esterification of oleic acid with methanol to produce biodiesel. Environmental Health Engineering and Management Journal 2023; 10(3): 321–329. doi: 10.34172/EHEM.2023.36.

**Article History:**
Received: 9 November 2022
Accepted: 12 March 2023
ePublished: 12 July 2023

***Correspondence to:**
Mohammad Rostamizadeh,
Email: Rostamizadeh@sut.ac.ir

## Introduction

Fossil fuels are the main source of energy in the world, which lead to serious environmental issues such as global warming, acidification of rain, and thinning of the ozone layer. Since fossil fuels are a limited energy source, increasing demand for energy forces to find an economically efficient and environmentally friendly alternative sources. In this regard, biodiesel as clean and renewable fuel, is a high potential candidate (1,2). A wide range of raw materials for biodiesel production including various categories of edible oils, non-edible oils, waste oils, animal fats, and algae oils has been identified (3,4). Biodiesel is defined as an oxygenated, sulfur-free, biodegradable, non-toxic, and environmentally friendly energy (1).

In general, biodiesel can be produced through esterification and/or transesterification of oil with alcohols (5,6). The heterogeneous alkali catalyst has high capacity to produce biodiesel, but it is not appropriate for feeds including free fatty acids (FFAs) and water. Also, homogeneous alkaline catalysts bring drawbacks such as non-reusability, soap production, difficult separation, and more wastewater (7). Therefore, heterogeneous acid catalysts have appealed a lot of consideration owing to addressing the mentioned drawbacks (7,8).

Zeolite imidazole framework-8 (ZIF-8) is a new class of crystalline porous materials and a subset of Metal-organic frameworks (MOFs), consisting of tetrahedral metal ions ($Zn^{2+}$) with imidazole binders. ZIF-8 has attracted a great deal of research as a heterogeneous catalyst due to its large surface area, adjustable pore size, chemical and structural stability, suitable capabilities, and most importantly hydrophobic properties (9,10). Saeedi et al (11) studied biodiesel production from soybean oil using modified k-Na/ZIF-8 catalyst in the transesterification process. They reported the conversion of 98% at methanol ratio of 10:1 and 3.5 hours. Narenji-Sani et al (12) prepared ZIF-like grafted $H_6P_2W_{18}O_{62}$ catalyst for the oleic acid esterification. The highest conversion was 92% in the optimum conditions, methanol ratio of 60:1, 3 wt.% catalyst, 80°C, and 4 hours. The conversion dropped to 19% after four sequence runs. Moatamed Sabzevar et al (13) applied $F_3O_4$@ZIF-8/$TiO_2$ catalyst in biodiesel production through the esterification of oleic acid. They found that the optimum operating conditions were 50 °C, methanol molar ratio of 30:1, 6 wt.% catalyst, and 62.5 minutes, resulting in the highest conversion (93%). Zhou et al (14) studied ZIF-8 in the oleic acid esterification at 130 °C, 10 wt.% catalyst, and 1 mL methanol. It is worth noting that catalyst with hydrophobic surfaces are desirable for biodiesel production because it prevents the adsorption of polar products such as water and glycerol in the reaction and increases the adsorption of hydrophobic components of the oil that causes a high conversion (15).

In this study, the nanocatalyst was prepared by the solvothermal technique and modified by sulfation process. The developed nanocatalyst was evaluated in the FFA esterification reaction to produce biodiesel. In addition, the impact of the operating conditions and reusability of the nanocatalyst were investigated.

## Materials and Methods

### Materials

The chemical materials were FFAs (palmitic (16%), oleic (66%), linoleic (15%)), zinc nitrate hexahydrate ($(Zn(No_3)_2.6H_2O$, 99%), 2-methylimidazole (Hmim, $C_4H_6N_2$, 98%), N,N-dimethylformamide (DMF, $C_3H_7NO$, 99%), ammonia ($NH_3$, 25% solution in water), methanol ($CH_3OH$, 99%), and sodium sulfate ($Na_2SO_4$, 98%) that were provided by Merck Company (Germany).

### Nanocatalyst preparation

The ZIF-8 nanocatalyst was synthesized with solvothermal technique at 25°C. The initial solution was prepared by zinc nitrate and ammonia. The second solution contained Hmim and DMF. The molar composition of the synthesis solution was $Zn^{2+}/Hmim/DMF/NH_3$: 1/2/41/30. After mixing the solutions, the final solution was converted to milky color and stirred at 25 °C for 6 hours. The mixture was then centrifuged and the obtained powder was washed three times with methanol. The drying process was carried out at 110 °C for 12 hours.

The sulfation process was performed with different ratios of 1M sodium sulfate solution to ZIF-8 nanocatalyst weight (4, 8, 16, and 24 cc $g^{-1}$) under reflux in an oil bath at 70 °C for 2 hours. Then, the reduction process was carried out by NaOH, deionized water, and $NaBH_4$. The solution was then stirred for 1 hour. Finally, the resulting solution was centrifuged and washed with deionized water. The modified nanocatalyst was dried in an oven at 110 °C for 12 hours. The modified nanocatalysts were denoted by XS where X indicated the ratio of sodium sulfate to ZIF-8 nanocatalyst weight.

### Characterization

Fourier transform infrared (FT-IR) spectra of zeolites were collected using Nexus Model Spectrophotometer (Nicolotco, USA) with the wavenumber of 400-4000 $cm^{-1}$. The field-emission scanning electron microscopy (FE-SEM) was performed by KYKY (Model, EM3200) device at a potential difference of 26 kV. Transmission electron microscopy (TEM) was performed on keV80 (Model, EM900) instrument. X-ray diffraction (XRD) was carried out with a D8 Advance Bruker AXS X-ray diffractometer with Ni-filter Cu Kα radiation. $N_2$ adsorption-desorption isotherms were studied at -196.2 °C (Quantachrome, USA). Temperature programed desorption of ammonia ($NH_3$-TPD Micromeritics, USA) with an on-line TCD detector evaluated acidity.

### Esterification reaction

The esterification reaction was performed in a Teflon-lined stainless-steel autoclave at different operating conditions: methanol to FFA molar ratio (5:1, 10:1, 20:1, and 40:1), amount of nanocatalyst (1, 3, 5, and 10 wt.%), reaction time (4, 6, 8, and 10 h), reaction temperature (100, 130, 160, and 190 °C), and stirring velocity of 700 rpm. At the end, the 0.1M KOH solution and phenolphthalein indicator were applied for the titration. The FFA conversion was calculated by Eq. (1).

$$\text{Conversion } (\%) = (V_i - V_f) / V_i \times 100 \quad (1)$$

where $V_i$ and $V_f$ are the volume of the applied KOH for titration of the feed and product, respectively.

## Results

### Effect of sulfation degree

The impact of sulfation degree was studied at four levels of the sodium sulfate to nanocatalyst ratio (4, 8, 16, and 24 cc $g^{-1}$). The operating conditions were the methanol to FFA molar ratio of 10:1, 10wt.% of nanocatalyst, temperature of 160 °C, and reaction time of 4 hours (Figure 1).

Figure 2 shows the XRD pattern of the nanocatalysts, including the ZIF-8 index peaks at $2\theta = 7.29$, 10.32, 12.65, 16.50, and 18.01°. The results confirm the correct synthesis of the ZIF-8 nanocatalysts based on the standard XRD pattern for the ZIF-8 (JCPDS: 00-035-0609) (16). It is also worth noting that the small difference in peak position and their crystallization intensity may result from the flexibility of the ZIF-8 structure (17). The lack of additional peaks confirms the appropriate sulfation process and homogeneous scattering of the sulfate groups. FT-IR spectrum of the nanocatalysts was recorded in the range of 400-4000 $cm^{-1}$ (Figure 3). The band at 3138 and 2933 $cm^{-1}$ can be assigned to the tensile vibrations of the C-H chain in the methyl group and the imidazole ring, respectively. The band at 1595 $cm^{-1}$ can be attributed to the C=N ring. The band in the range of 1100-1400 $cm^{-1}$ can be attributed to the C-H ring. The bands in 900-1100 $cm^{-1}$ are related to the C-N stretching vibrations and the band at 421 $cm^{-1}$ is assigned to the Zn-N tensile vibrations (18,19). The band at 588 $cm^{-1}$ is assigned to the sulfate groups (20), confirming the sulfation process.

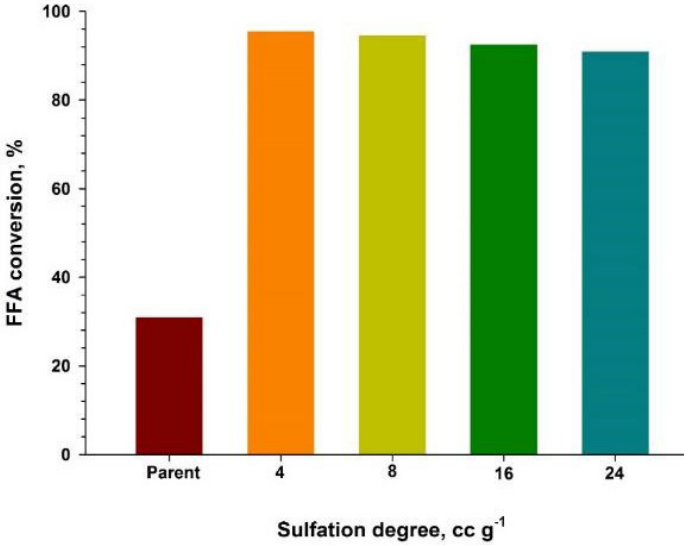

**Figure 1.** Effect of sulfation degree on the FFA conversion. Reaction conditions: methanol molar ratio of 10:1, 10 wt.% catalyst, temperature of 160°C, and reaction time of 4 h

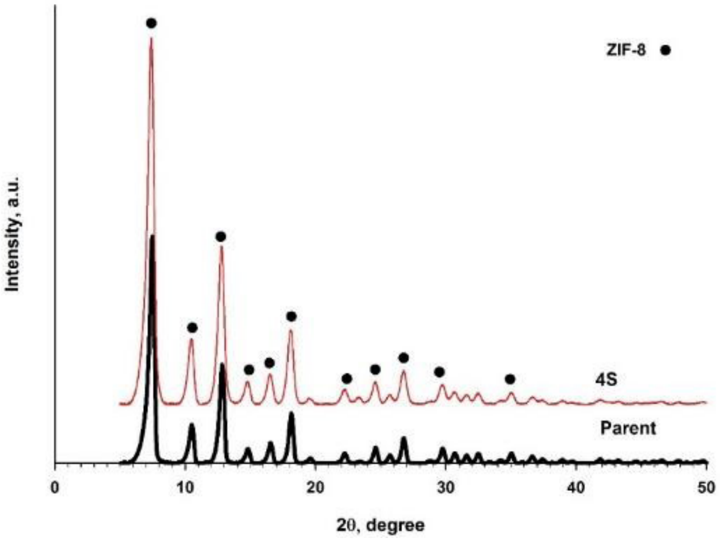

**Figure 2.** XRD pattern of the parent and 4S nanocatalysts

FE-SEM and TEM images show that morphology of the parent and 4S nanocatalysts includes spherical shape and scattered particles (Figure 4), which is consistent with the literature (16). Figure 5 shows the textural data of the nanocatalysts. The results show that the sulfate group loading decreases the surface area from 1313.6 to 995.6 $m^2g^{-1}$. The reduction of the surface area of the 4S nanocatalyst can be explained by slight framework destruction. According to the IUPAC classification, the nanocatalysts show a type IV Langmuir isotherm that is related to the porous structure (Figure 5a). The high absorption volume at the low relative pressure of $P/P_0 < 0.2$ indicates a microporous structure (16,21). The average pore diameter of the parent and 4S nanocatalysts was 1.73 and 1.74 nm, respectively, indicating the impact of the sulfate groups on the pore structure. Furthermore, the Barrett-Joyner-Halenda (BJH) results confirm the mesopore structure of the 4S nanocatalyst (Figure 5b). The large pore size favors the low mass transfer resistance and the high performance in the biodiesel production. Figure 6 shows the $NH_3$-TPD results for the nanocatalysts. The density of the acid sites can be determined by the peak area and the strength of the acid sites is specified by the location of the peaks. The first peak represents the weak acid sites and the second one represents the strong acid sites. The two desorption peaks in the temperature range of 102 °C and 335 °C reveal the weak and strong acidic sites of the parent nanocatalyst, respectively. The 4S nanocatalyst has two desorption peaks at 321°C and 379 °C, showing the huge strong acidity. The sulfation enhances the strong acid sites and decreases the number of the weak acid sites (22). Furthermore, the higher peak

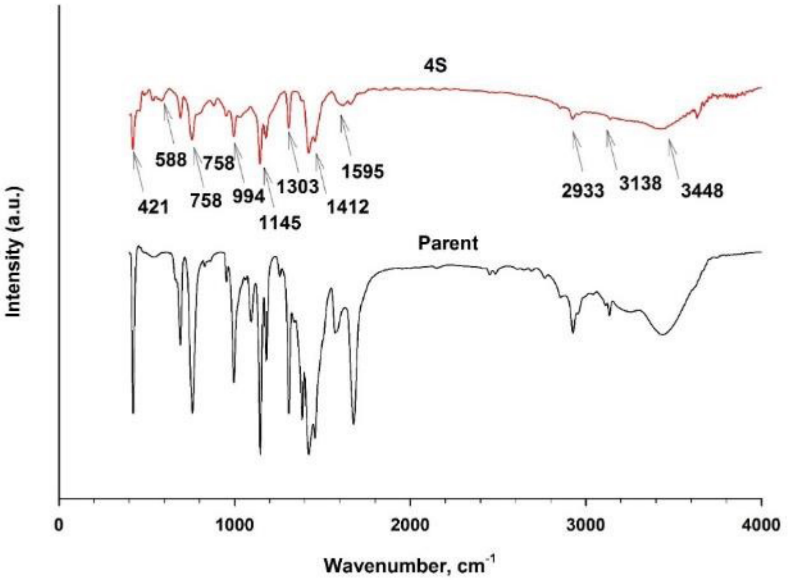

**Figure 3.** FT-IR spectrum of the parent and 4S nanocatalysts

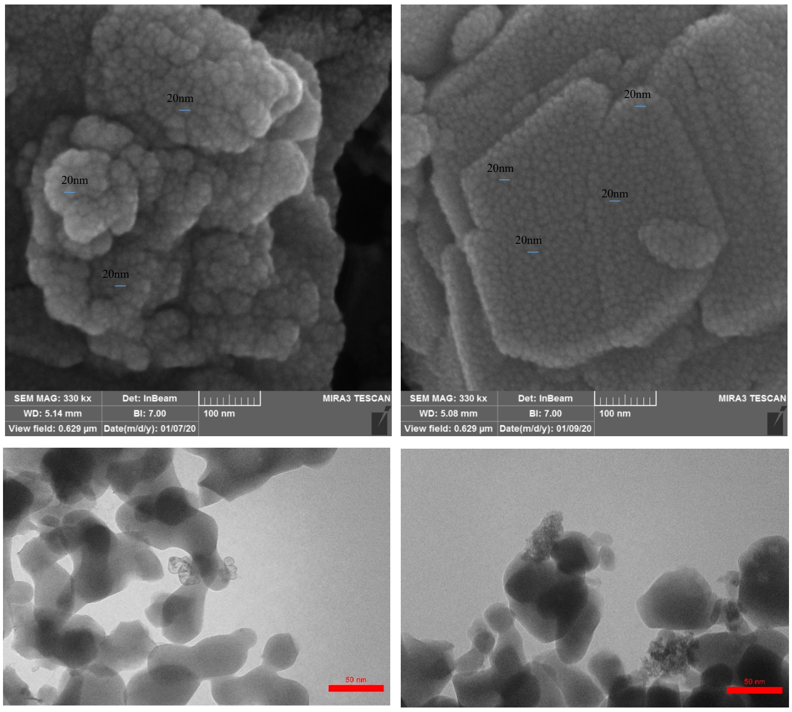

**Figure 4.** FE-SEM and TEM images of the nanocatalysts: Parent (left) and 4S (right)

temperature of the second peak indicates the higher strength of the acid sites for the 4S nanocatalyst compared with the parent nanocatalyst.

### *The impact of the nanocatalyst amount*

The esterification reaction over the 4S nanocatalyst was studied using different levels of the nanocatalyst (1, 3, 5, and 10 wt.%) and the following conditions: methanol ratio of 10:1, temperature of 160 °C, and reaction time of 4 hours (Figure 7a). The increase of the nanocatalyst concentration (up to 3 wt.%) enhances the FFA conversion (up to 96%).

### *The impact of reaction time*

The progressive of the esterification reaction over the 4S nanocatalyst was studied at different reaction times (4, 6, 8, and, 10 hours) at the following reaction conditions: methanol ratio of 10:1, 3wt.% nanocatalyst, and temperature of 160 °C (Figure 7b).

### *The impact of temperature*

It is believed that temperature significantly influences the catalytic activity and reaction progress, especially in the equilibrium reaction like esterification. The effect of temperature on the esterification over the 4S nanocatalyst was investigated at different temperatures (100, 130, 160 and, 190 °C) and the following conditions: methanol molar ratio of 10:1, 3 wt.% nanocatalyst, and reaction time of 6 hours (Figure 7c).

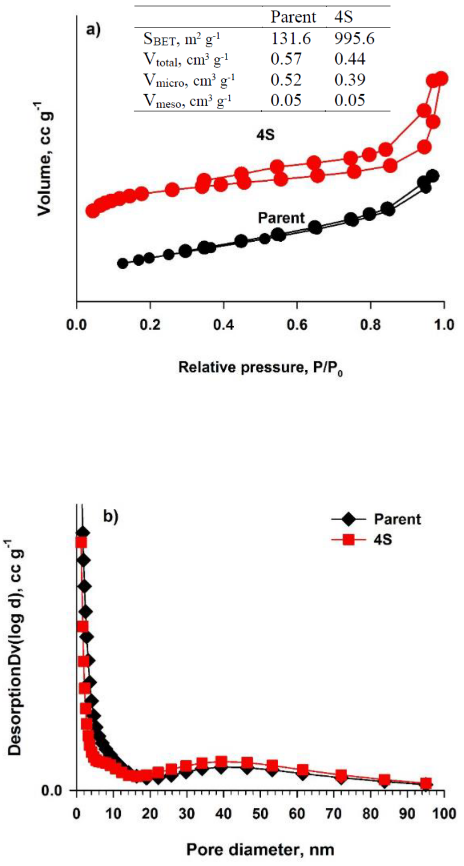

| | Parent | 4S |
|---|---|---|
| $S_{BET}$, m$^2$ g$^{-1}$ | 131.6 | 995.6 |
| $V_{total}$, cm$^3$ g$^{-1}$ | 0.57 | 0.44 |
| $V_{micro}$, cm$^3$ g$^{-1}$ | 0.52 | 0.39 |
| $V_{meso}$, cm$^3$ g$^{-1}$ | 0.05 | 0.05 |

**Figure 5.** (a) $N_2$ adsorption-desorption isotherm and (b) BJH pore size distribution of the parent and 4S nanocatalysts

### *The impact of methanol ratio*

This parameter was studied at different methanol molar ratios (5:1, 10:1, 20:1, and 40:1) and the following conditions: 3 wt.% nanocatalyst, temperature of 160 °C, and reaction time of 6 h (Figure 7d).

### *The reusability*

The reusability of the 4S nanocatalyst was studied. After each run, the spent nanocatalyst was recovered from the products. Then, it was washed twice with n-hexane and dried for 12 hours in an oven at 110 °C. The reusability was evaluated at the obtained optimal conditions (methanol ratio of 10:1, 3 wt.% nanocatalyst, 160 °C, and 6 hours). Figure 8 shows the high stability and catalytic activity of the 4S nanocatalyst through the several cycles of the esterification reaction.

Figure 9 shows the characterization results of the used 4S nanocatalyst, which includes the index XRD peaks related to the ZIF-8 structure.

## Discussion

### *Effect of sulfation degree*

The results show that the 4S nanocatalyst results in the best performance and the high conversion of 95.5%, which represents a significant improvement compared the FFA conversion (31%) over the parent nanocatalyst. This result can be explained by the formation of an appropriate acidic intensity and density on the nanocatalyst through the sulfation process. Furthermore, it is reported that sulfation improved the hydrophobicity of the surface (22), enhancing the adsorption of the FFA molecules as well as the desorption of the produced water over the 4S nanocatalyst through the esterification reaction. It is worth noting that the higher sulfation degrees (>4)

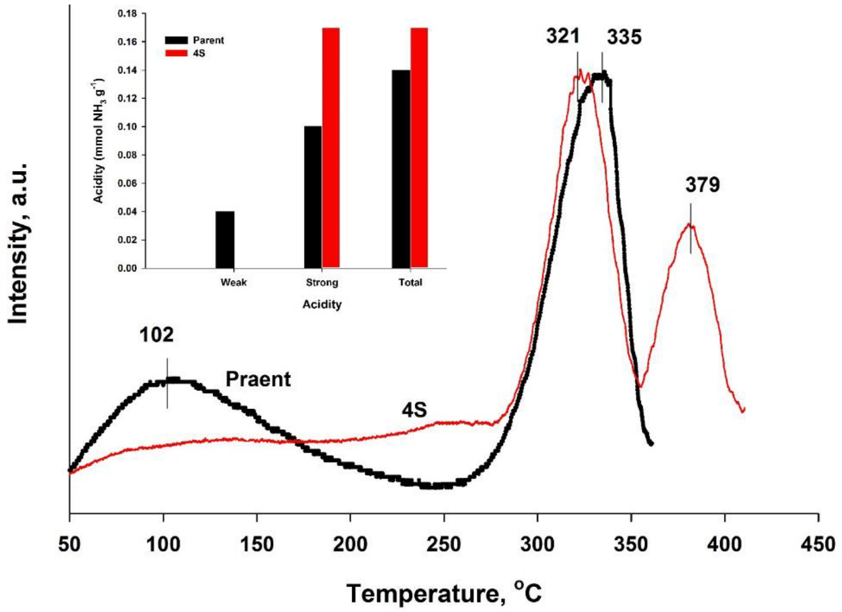

**Figure 6.** $NH_3$-TPD results of the parent and 4S nanocatalysts

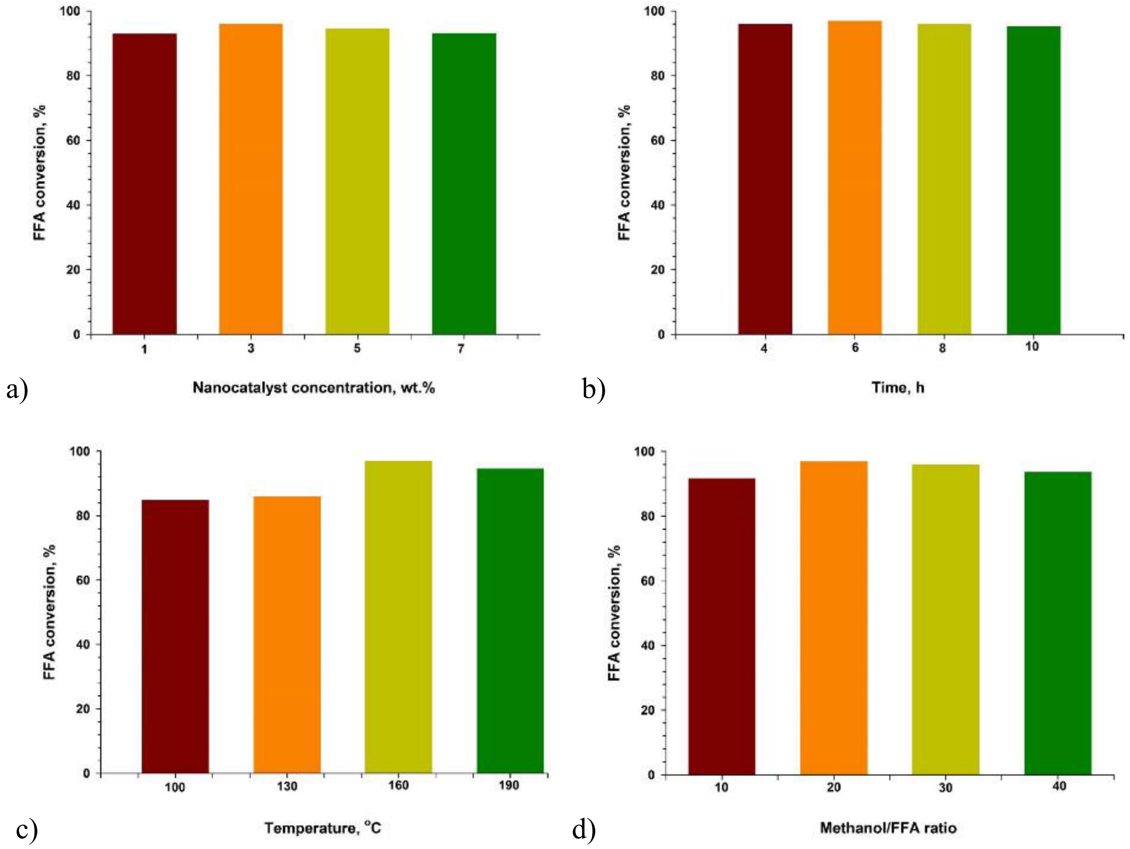

**Figure 7.** Effect of operating conditions, (a) nanocatalyst concentration; (b) time; (c) temperature; (d) methanol/FFA ratio, on the FFA conversion

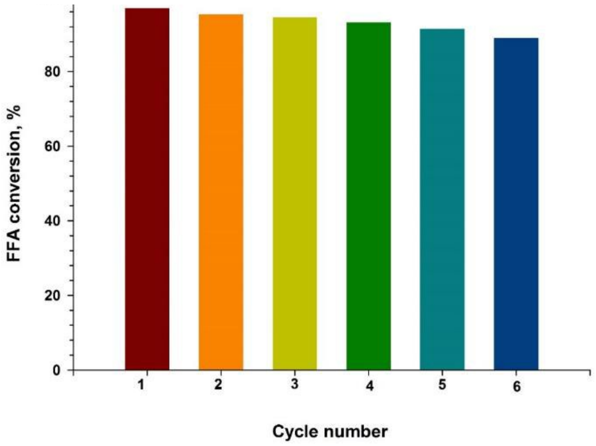

**Figure 8.** The reusability of the 4S nanocatalyst. Reaction conditions: methanol molar ratio of 10:1, 3 wt.% nanocatalyst, temperature of 160°C, and reaction time of 6 h

reduce the accessibility of the acidic sites due to pore blockage, leading to the low FFA conversion. Therefore, the sodium sulfate to nanocatalyst ratio of 4 is the optimal ratio for loading the sulfate groups.

### *The impact of the nanocatalyst amount*

The results can be explained by more active sites and the appropriate contact between the feed and nanocatalyst, which is consistent with the results reported in the literature (23,24). However, more increase of the nanocatalyst amount (10 wt.%) decreases the FFA conversion (93%) because of the increased viscosity of the mixture and the limitation of penetration. Furthermore, the excess nanocatalyst disrupts the reaction because the required amount of nanocatalyst is proportional to the amount of reactant (25,26). Thus, the optimum nanocatalyst amount for the esterification reaction over the 4S nanocatalyst is 3 wt.%.

### *The impact of reaction time*

The long-time reaction (6 hours) increases the high FFA conversion (97%) owing to the sufficient feed-nanocatalyst contact. But, the longer reaction time (10 hours) reduces the FFA conversion (95%). It is accepted that the esterification reaction is reversible and very long time of reaction leads to the backward reaction and the reduction of the FFA conversion. Narenji-Sani et al. (12) reported that oleic acid conversion over the ZIF-like Grafted $H_6P_2W_{18}O_{62}$ catalyst did not change after 6 hours owing to the equilibrium. Therefore, 6 h is selected as the optimum reaction time over the 4S nanocatalyst.

### *The impact of temperature*

The results show that the FFA conversion increases with temperature. The highest conversion (97%) is obtained

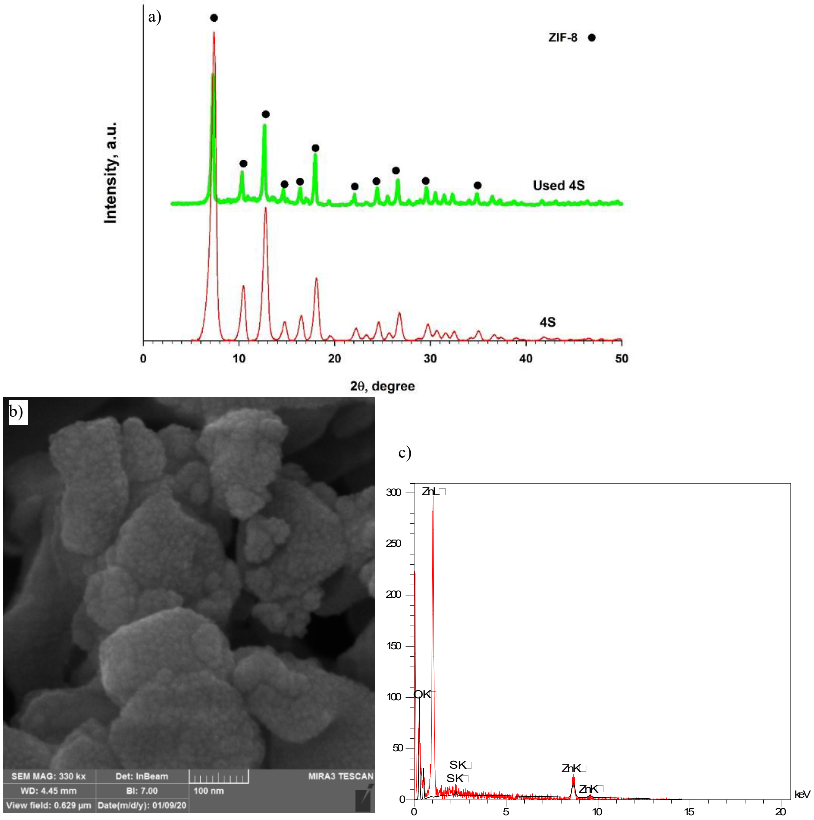

**Figure 9**. The characterization of the used 4S nanocatalyst (a) XRD, (b) FE-SEM, and (c) EDX

at 160 °C. This phenomenon can be explained by the endothermic nature of the esterification reaction, leading to the more forward reaction by temperature increasing. It is accepted that the high reaction temperature favors the low viscosity of reaction solution, and so the low mass transfer resistance between feed and nanocatalyst, improving the FFA conversion (27). However, more increase of temperature (190 °C) reduces the FFA conversion (94%) due to the equilibrium. Thus, temperature of 160 °C is selected as the optimum temperature for the esterification over the 4S nanocatalyst.

### *The impact of methanol ratio*

The esterification is a reversible reaction and its stoichiometric molar ratio for methanol and fatty acid is 1:1. According to the Le Chatelier principal, extra methanol forces the reaction to progress toward the products, and also, minimizes the backward reaction. The highest conversion (97%) is obtained at the methanol ratio of 10:1. The increase of methanol molar ratio (40:1) reduces the FFA conversion (94%) owing to the competitive adsorption of methanol and FFA molecules on the nanocatalyst surface. Furthermore, the high methanol molar ratio results in the low nanocatalyst concentration in the reaction medium, the low contact between feed and nanocatalyst, and the low conversion (28). So, the methanol ratio of 10:1 is the optimum ratio for the esterification reaction.

### *The reusability*

From economic point of view, the development of a long-term and high-efficient nanocatalyst can significantly influence biodiesel production. Surprisingly, the FFA conversion drops only 8% after six sequence runs, indicating the suitable structural and physic-chemical properties of the developed nanocatalyst. It is accepted that the active phase leaching is one of the most important factors through the reusability, which reduces the catalytic activity. The development of the 4S nanocatalyst and incorporation of the sulfate active phase on the parent structure addresses the leaching issues, resulting in the durable and long lifetime for the nanocatalyst in the esterification reaction. Obviously, this achievement can significantly affect the economical aspect of the biodiesel production. The results confirm the high stability of the nanocatalyst without significant framework destructions through the experiments that are consistent with the reusability results. However, the intensity of the index peaks is reduced for the used nanocatalyst due to the deactivation of the active phase. The FE-SEM image of the used 4S nanocatalyst represents no significant change in the morphology, size, and shape of the particles through

**Table 1.** Comparison between performances of different catalysts in the biodiesel production

| Catalyst | Feedstock | Catalyst Amount, wt.% | Alcohol to Oil Ratio | Temperature (℃) | Conversion (%) | Ref. |
|---|---|---|---|---|---|---|
| ZIF-8 | Oleic acid | 1 | - | 130 | 88 | (14) |
| $Fe_3O_4$@ZIF-8/$TiO_2$ | Oleic acid | 6 | 30 | 50 | 80 | (13) |
| $Fe_3O_4$@ZIF-8/$TiO_2$ | Oleic acid | 6 | 30 | 50 | 92 | (13) |
| $H_6P_2W_{18}O_{62}$/ZIF-8 | Oleic acid | 3 | 60 | 80 | 92 | (12) |
| 4S | Oleic acid | 3 | 10 | 160 | 97 | This work |

the esterification reaction (Figure 9b), which supports the XRD results as well as the high stability through the sequence runs.

Table 1 compares the reported performance of the different catalysts in the literature and the present study. As shown in this table, the developed 4S nanocatalyst had the highest conversion. The high performance of the developed nanocatalyst can be resulted from the well-adjusted properties. The key benefits of the 4S nanocatalyst are the low amount of the required catalyst, low methanol ratio, and high reusability. From industrial point of view, these can reduce the size of equipment and energy requirements.

## Conclusion

In this study, biodiesel production using the modified MOF nanocatalyst was investigated in the esterification reaction. The synthesis of the nanocatalyst was carried out with the solvothermal method at 25 °C, which was modified through sulfation process. The nanocatalyst characterization showed the high crystallinity, high surface area, appropriate acidity, and homogeneous dispersion of the active sites. The highest FFA conversion was obtained over the nanocatalyst with the low sulfation degree in the following operating conditions: methanol to FFA ratio of 10:1, 3 wt.% nanocatalyst, 6 hours, and 160 °C. Surprisingly, the 4S nanocatalyst exhibited a high reusability and a low FFA conversion drop through six sequence runs. These results proved the high capability of the developed nanocatalyst in the esterification reaction to produce biodiesel.

## Acknowledgements

The authors would like to thank Sahand University of Technology for their support.

## Authors' contribution

**Conceptualization:** Mohammad Rostamizadeh.
**Data curation:** Mahsa Oghabi.
**Formal analysis:** Mahsa Oghabi.
**Funding acquisition:** Mohammad Rostamizadeh.
**Investigation:** Mahsa Oghabi.
**Methodology:** Mohammad Rostamizadeh.
**Project administration:** Mohammad Rostamizadeh.
**Resources:** Mahsa Oghabi.
**Software:** Mahsa Oghabi.
**Supervision:** Mohammad Rostamizadeh.
**Validation:** Mahsa Oghabi.
**Visualization:** Mahsa Oghabi.
**Writing–original draft:** Mahsa Oghabi.
**Writing–review & editing:** Mohammad Rostamizadeh.

## Competing interests

The authors declare that they have no conflict of interests.

## Ethical issues

It is hereby declared that this work and the obtained results are the original experimental work of the authors and it has neither been published, nor is it under review in another journal, and it is not being submitted for publication in any other journals.

## References

1. Rahmani Vahid B, Saghatoleslami N, Nayebzadeh H, Toghiani J. Effect of alumina loading on the properties and activity of SO42−/ZrO2 for biodiesel production: process optimization via response surface methodology. J Taiwan Inst Chem Eng. 2018;83:115-23. doi: 10.1016/j.jtice.2017.12.007.
2. Jadav D, Bandyopadhyay R, Bandyopadhyay M. Synthesis of hierarchical SAPO-5 & SAPO-34 materials by post-synthetic alkali treatment and their enhanced catalytic activity in transesterification. Eur J Inorg Chem. 2020;2020(10):847-53. doi: 10.1002/ejic.201901250.
3. Elystia S, Muria SR, Erlangga HF. Cultivation of *Chlorella pyrenoidosa* as a raw material for the production of biofuels in palm oil mill effluent medium with the addition of urea and triple super phosphate. Environ Health Eng Manag. 2020;7(1):1-6. doi: 10.34172/ehem.2020.01.
4. Maheshwari P, Haider MB, Yusuf M, Klemeš JJ, Bokhari A, Beg M, et al. A review on latest trends in cleaner biodiesel production: role of feedstock, production methods, and catalysts. J Clean Prod. 2022;355:131588. doi: 10.1016/j.jclepro.2022.131588.
5. Boffito DC, Blanco Manrique G, Patience GS. One step cracking/transesterification of vegetable oil: reaction–regeneration cycles in a capillary fluidized bed. Energy Convers Manag. 2015;103:958-64. doi: 10.1016/j.enconman.2015.07.025.
6. Malakootian M, Hatami B, Dowlatshahi S, Rajabizadeh A. Growth and lipid accumulation in response to different cultivation temperatures in *Nannochloropsis oculata* for biodiesel production. Environ Health Eng Manag. 2016;3(1):29-34.
7. Sun K, Lu J, Ma L, Han Y, Fu Z, Ding J. A comparative study on the catalytic performance of different types of zeolites for biodiesel production. Fuel. 2015;158:848-54. doi: 10.1016/j.fuel.2015.06.048.

8. Nandiwale KY, Sonar SK, Niphadkar PS, Joshi PN, Deshpande SS, Patil VS, et al. Catalytic upgrading of renewable levulinic acid to ethyl levulinate biodiesel using dodecatungstophosphoric acid supported on desilicated H-ZSM-5 as catalyst. Appl Catal A Gen. 2013;460-461:90-8. doi: 10.1016/j.apcata.2013.04.024.
9. Reinsch H. "Green" synthesis of metal-organic frameworks. Eur J Inorg Chem. 2016;2016(27):4290-9. doi: 10.1002/ejic.201600286.
10. Percástegui EG. Guest-induced transformations in metal-organic cages. Eur J Inorg Chem. 2021;2021(43):4425-38. doi: 10.1002/ejic.202100657.
11. Saeedi M, Fazaeli R, Aliyan H. Nanostructured sodium–zeolite imidazolate framework (ZIF-8) doped with potassium by sol–gel processing for biodiesel production from soybean oil. J Solgel Sci Technol. 2016;77(2):404-15. doi: 10.1007/s10971-015-3867-1.
12. Narenji-Sani F, Tayebee R, Chahkandi M. New task-specific and reusable ZIF-like grafted H6P2W18O62 catalyst for the effective esterification of free fatty acids. ACS Omega. 2020;5(17):9999-10010. doi: 10.1021/acsomega.0c00358.
13. Moatamed Sabzevar A, Ghahramaninezhad M, Niknam Shahrak M. Enhanced biodiesel production from oleic acid using TiO2-decorated magnetic ZIF-8 nanocomposite catalyst and its utilization for used frying oil conversion to valuable product. Fuel. 2021;288:119586. doi: 10.1016/j.fuel.2020.119586.
14. Zhou K, Chaemchuen S. Metal-organic framework as catalyst in esterification of oleic acid for biodiesel production. Int J Environ Sci Dev. 2017;8(4):251-4. doi: 10.18178/ijesd.2017.8.4.957.
15. Khan NA, el Dessouky H. Prospect of biodiesel in Pakistan. Renew Sustain Energy Rev. 2009;13(6-7):1576-83. doi: 10.1016/j.rser.2008.09.016.
16. Thi Thanh M, Vinh Thien T, Thi Thanh Chau V, Dinh Du P, Phi Hung N, Quang Khieu D. Synthesis of iron doped zeolite imidazolate framework-8 and its Remazol Deep Black RGB dye adsorption ability. J Chem. 2017;2017:5045973. doi: 10.1155/2017/5045973.
17. Stoyanova A, Iordanova R, Mancheva M, Dimitriev Y. Synthesis and structural characterization of MoO3 phases obtained from molybdic acid by addition of HNO3 and H2O2. J Optoelectron Adv Mater. 2009;11(8):1127-31.
18. Tran UP, Le KK, Phan NT. Expanding applications of metal–organic frameworks: zeolite imidazolate framework ZIF-8 as an efficient heterogeneous catalyst for the Knoevenagel reaction. ACS Catal. 2011;1(2):120-7. doi: 10.1021/cs1000625.
19. Shetty M, Murugappan K, Prasomsri T, Green WH, Román-Leshkov Y. Reactivity and stability investigation of supported molybdenum oxide catalysts for the hydrodeoxygenation (HDO) of m-cresol. J Catal. 2015;331:86-97. doi: 10.1016/j.jcat.2015.07.034.
20. Bhattacharyya S, Pang SH, Dutzer MR, Lively RP, Walton KS, Sholl DS, et al. Interactions of SO2-containing acid gases with ZIF-8: structural changes and mechanistic investigations. J Phys Chem C. 2016;120(48):27221-9. doi: 10.1021/acs.jpcc.6b09197.
21. Gao C, Chen S, Quan X, Yu H, Zhang Y. Enhanced Fenton-like catalysis by iron-based metal organic frameworks for degradation of organic pollutants. J Catal. 2017;356:125-32. doi: 10.1016/j.jcat.2017.09.015.
22. Lowe B, Gardy J, Hassanpour A. The role of sulfated materials for biodiesel production from cheap raw materials. Catalysts. 2022;12(2):223. doi: 10.3390/catal12020223.
23. Gan S, Ng HK, Chan PH, Leong FL. Heterogeneous free fatty acids esterification in waste cooking oil using ion-exchange resins. Fuel Process Technol. 2012;102:67-72. doi: 10.1016/j.fuproc.2012.04.038.
24. Srilatha K, Sree R, Prabhavathi Devi BLA, Sai Prasad PS, Prasad RBN, Lingaiah N. Preparation of biodiesel from rice bran fatty acids catalyzed by heterogeneous cesium-exchanged 12-tungstophosphoric acids. Bioresour Technol. 2012;116:53-7. doi: 10.1016/j.biortech.2012.04.047.
25. Wu H, Zhang J, Wei Q, Zheng J, Zhang J. Transesterification of soybean oil to biodiesel using zeolite supported CaO as strong base catalysts. Fuel Process Technol. 2013;109:13-8. doi: 10.1016/j.fuproc.2012.09.032.
26. Moradi GR, Dehghani S, Ghanei R. Measurements of physical properties during transesterification of soybean oil to biodiesel for prediction of reaction progress. Energy Convers Manag. 2012;61:67-70. doi: 10.1016/j.enconman.2012.03.015.
27. Ma X, Liu F, Helian Y, Li C, Wu Z, Li H, et al. Current application of MOFs based heterogeneous catalysts in catalyzing transesterification/esterification for biodiesel production: a review. Energy Convers Manag. 2021;229:113760. doi: 10.1016/j.enconman.2020.113760.
28. Alismaeel ZT, Abbas AS, Albayati TM, Doyle AM. Biodiesel from batch and continuous oleic acid esterification using zeolite catalysts. Fuel. 2018;234:170-6. doi: 10.1016/j.fuel.2018.07.025.